CHANGE DETECTION METHODS FOR RADAR IMAGES
An overview of promising methods

I.C. SIKANETA
IAEA
Vienna, Austria
Email: i.sikaneta@iaea.org

A.N. LARSON
IAEA
Vienna, Austria

Abstract

Change-detection analysis of radar imagery can indicate subtle change, for example, it can reveal tracks of disturbed earth that can be associated with vehicle movements across unpaved roads in the period between collection of the two images. Identifying changes of interest in radar imagery is challenging, and thus difficult to automate, because these changes of interest must be differentiated from changes due to instrument effects, scattering effects (speckle), variations in backscatter (scattering from features of different type or shadow), image-processing effects and background environmental variations. The paper has three goals: (1) describe change-detection methods for radar data with attention given to confidence measures, (2) describe some of the types of changes that radar can detect, and (3) illustrate the performance of change detection algorithms, including results from a new statistical change detection algorithm and a supervised Machine Learning (ML) algorithm.

1. INTRODUCTION

Satellite radar imagery provides several niche indicators of activity related to the Nuclear Fuel Cycle (NFC). Along with the capability to image objects, such as equipment, vehicles, material and buildings, independent of cloud-cover or daylight, radar imagery possesses a unique capability (among remote sensing technologies) to identify areas of subtle physical change. By using the technique of Coherent Change Detection (CCD) it can, for instance, identify the small changes in the distribution of gravel, sand or soil resulting from the use of a vehicle upon a track, or the centimetre-level variations in position or orientation of equipment that has been moved or used.

Identifying and interpreting changes of relevance presents a significant challenge to radar imagery analysis. Among the peculiarities of radar imagery are the effects of layover, shadow and speckle, each of which can produce signatures that resemble true physical changes of interest. These effects can be further aggravated by non-ideal properties of the sensing instrument. For instance, critical to identifying CCD signatures is the requirement that images are collected on a so-called repeat-pass orbit meaning the satellite follows exactly the same trajectory, relative to the scene, when creating the images that are to be compared. If the trajectory match is not perfect, spurious layover effects on the CCD image start to resemble signatures of real interest.

Compounding the challenge of identifying change using radar imagery is the fact that, nowadays, there is a lot of radar imagery available. The European Space Agency (ESA) shares cost-free radar imagery through its Sentinel-1 mission which operates on a plan to image almost every location on the earth on at least a 12-day repeat pass cycle. Obtaining, processing and analysing Sentinel-1 imagery over sites of interest requires a significant level of effort, especially because the radar images cover several hundreds of square kilometres. In an operational environment, these Sentinel-1 data would only be part of a larger set of radar imagery from commercial vendors.

Motivated by the large volume of data and the challenges of performing the analysis, this paper discusses methods for automating change detection using radar imagery. It reviews and illustrates two methods , [1,2,6], published in open literature, one of which, [2], has been coded into software named MIMOSA. Additionally, it presents a new approach, which extends these methods. Finally, it discusses how machine learning methods might be applied.

The next section reviews the model that serves as a basis for these automatic change detection algorithms. This is followed by a section discussing how one might enhance these methods. The final section

discusses the use of machine learning methods and provides an example of a machine learning technique applied to Synthetic Aperture Radar (SAR) imagery to help eliminate false change over a region of interest. From here onwards we refer to radar and SAR interchangeably.

2. THE MODEL FOR AUTOMATIC CHANGE DETECTION ALGORITHMS

The following outlines the statistical model for comparing radar imagery. References [1,2,4,6,7] are all based upon this model.

Two statistically independent processes contribute to the value of the radar dataset at any location. The first, called a noise process, is a white, circular, stationary Gaussian thermal noise contribution which is unavoidable for any measurement system. The second process, called a clutter process, is also modelled as a circular Gaussian process, neither white nor stationary, and arises from the physical reflection of coherent radar waves from multiple, randomly-distributed scatterers, [6]. With the assumption that reflections from these scatterers are identically distributed (statistically), then invocation of the central limit theorem leads to a Gaussian distribution for the coherent sum of their reflections. Because it is a coherent imaging system, the raw radar data values are complex numbers with amplitudes related to the reflectivity of the scatterers and phases related to the distance of the scatters from the radar satellite. A precise measurement of the phase provides the mechanism for detecting centimetre-level changes.

Since the amplitude of the signal is related to the reflectivity of the scatterers, and since a radar dataset may cover regions with various types of scatterers, (e.g. desert, sparse brush, grass, e.t.c) the clutter process cannot be considered spatially stationary in its variance. If (m, n) denotes the coordinates of a point in a set of co-registered datasets, then the radar values can be represented as

$$\vec{z}(m,n) = \vec{c}(m,n) + \vec{v}(m,n)$$

where $\vec{z}(m,n)$ is a column vector with elements given by the dataset value at position (m,n) for each dataset in the set of radar collections. The vector $\vec{c}(m,n)$ represents the clutter signal while $\vec{v}(m,n)$, represents the thermal noise contribution. The signal to noise ratio SNR is given by the ratio of their mean square-amplitudes. If M radar datasets are to be analysed, then the vector will have M elements. The question to be answered is whether, statistically, each element of $\vec{z}(m,n)$ is of the same type, or if there is at least one element that is different. If there is one element that is different, then there is a change detected at coordinates (m,n).

Because the amplitude is a reflection of the intensity of scattering, a radar image is oftentimes, created by mapping the complex values of the measurement to a real number. In the case of multiple radar datasets, one approach to creating imagery proceeds as follows: First a matrix is defined by arranging the vectors covered by a given window centred at (m', n'):

$$\boldsymbol{Z}(m',n') = [\alpha_{00}\vec{z}(m_0,n_0) \;\; \alpha_{10}\vec{z}(m_1,n_0) \;\; \alpha_{20}\vec{z}(m_2,n_0) \ldots]$$

for each set of indices (m_i, n_j) covered by the window and weighted by the window coefficients: α_{ij}. One then computes

$$\widehat{\boldsymbol{R}}(m',n') = \boldsymbol{Z}(m',n')\boldsymbol{Z}^H(m',n')$$

where $.^H$ denotes Hermitian transpose.

Each diagonal element of $\widehat{\boldsymbol{R}}(m',n')$ is a real number and represents a filtered (by the window) version of one radar image in the set. The complex off-diagonal elements represent estimates of the cross-correlation between images and when appropriately normalised, yield a value between 0 and 1 indicating a statistical measure of similarity between each pair of radar datasets.

2.1. Statistical Change detection

The challenge is to determine whether the matrix $\widehat{\boldsymbol{R}}(m',n')$ represents a location of change. In an approach called Constant False Alarm Rate (CFAR) detection, one computes the joint probability distribution of

some appropriately chosen set of functions of the elements of $\widehat{\boldsymbol{R}}(m',n')$ under the assumption that there has been no change. With knowledge of the distribution function, one then identifies a region in the space of the output of this set of functions such that the probability of a value falling into this region is given by the so-called false alarm probability.

As a specific example, we examine how MIMOSA uses the diagonal elements of $\widehat{\boldsymbol{R}}(m',n')$ to create a test statistic for change detection. By denoting the diagonal elements as $x_1^2, x_2^2, x_3^2, \dots, x_M^2$, the algorithm computes generalized mean values from $x_1, x_2, x_3, \dots, x_M$. In particular, means given by

$$m_0 = \sqrt[M]{x_1 x_2 \dots x_M}$$

$$m_k = \left(\frac{1}{M}\sum_{i=1}^{M} x_i^k\right)^{\frac{1}{k}}$$

are computed and ratios given by $T = m_k/m_l$, for some k and l, are calculated. To be more precise, $T = T(m',n')$ and can be arranged into a matrix representing an image. By considering $T(m',n')$ as a realization of a random variable, and with knowledge of the distribution of this variable (which, ideally, can be calculated), a threshold can be computed such that $T(m',n')$ exceeds the threshold with probability given by a desired false alarm probability.

References [1] and [6] apply what can be shown to be a similar technique by computing and comparing functions of the determinants of blocks of $\widehat{\boldsymbol{R}}(m',n')$.

3. A NEW STATISTICAL CHANGE DETECTION METHOD

This section presents a new proposal for statistical change detection. It is a variation on previous methods statistical and applies to the specific case of trying to identify changes in a pair of radar images.

3.1. Joint coherent and amplitude change detection

In the case of two radar images, one may write $\widehat{\boldsymbol{R}}(m',n')$ as

$$\widehat{\boldsymbol{R}}(m',n') = \begin{bmatrix} x_1^2(m',n') & |x_1(m',n')x_2(m',n')|\hat{\rho}(m',n')e^{i\theta(m',n')} \\ |x_1(m',n')x_2(m',n')|\hat{\rho}(m',n')e^{-i\theta(m',n')} & x_2^2(m',n') \end{bmatrix}$$

where $\hat{\rho}(m',n') \in [0,1]$ and where $\theta(m',n')$ is some phase. The well know radar CCD image is created by calculating $\hat{\rho}(m',n')$, also known as the coherence or correlation coefficient, at all values (m',n').

As already mentioned, this correlation coefficient is sensitive to centimeter-level changes between the radar images. Values of $\hat{\rho}(m',n')$ close to zero indicate coherent change between images. One also knows that if an object has appeared or disappeared from a location (m',n'), then its amplitude responses $x_1^2(m',n')$ and $x_2^2(m',n')$ will be different. The objective of this subsection is to combine amplitude and coherent change detection.

Consider a pair of random variables given by $T_1(m',n'), T_2(m',n')$ with

$$T_1(m',n') = \frac{x_1^2(m',n')}{x_1^2(m',n') + x_2^2(m',n')}$$

$$T_2(m',n') = \hat{\rho}(m',n')$$

If the image amplitude responses are the same or similar, then $T_1(m',n')$ will be close to a half. Notable amplitude changes cause the test statistic to take values either close to zero or close to one. Note that, like $T_2(m',n')$, $T_1(m',n') \in [0,1]$. As illustrated in FIG 1, the joint probability distribution function for this pair of random variables can be calculated under the assumptions of the model of Section 2. The joint probability distribution for the proposed method has been calculated through mathematical manipulation of the material in [7] with a final result given by

$$f_{T_1,T_2}(T_1,T_2) = 4^n[T_1(1-T_1)]^{n-1}T_2(1-T_2^2)^{n-2}(1-\rho^2)^n \frac{\Gamma\left(n+\frac{1}{2}\right)}{\sqrt{\pi}\Gamma(n-1)} \; {}_2F_1\left(n, n+\frac{1}{2}; 1; 4T_1[1-T_1]\rho^2T_2^2\right)$$

where ${}_2F_1(a,b;c;x)$ and $\Gamma(z)$ denote, respectively, the Gauss hypergeometric and gamma functions, [8]. The parameters ρ and n denote the true underlying correlation coefficient and the effective number of looks, [7]. Examples of this distribution are illustrated of FIG 1 and FIG 2.

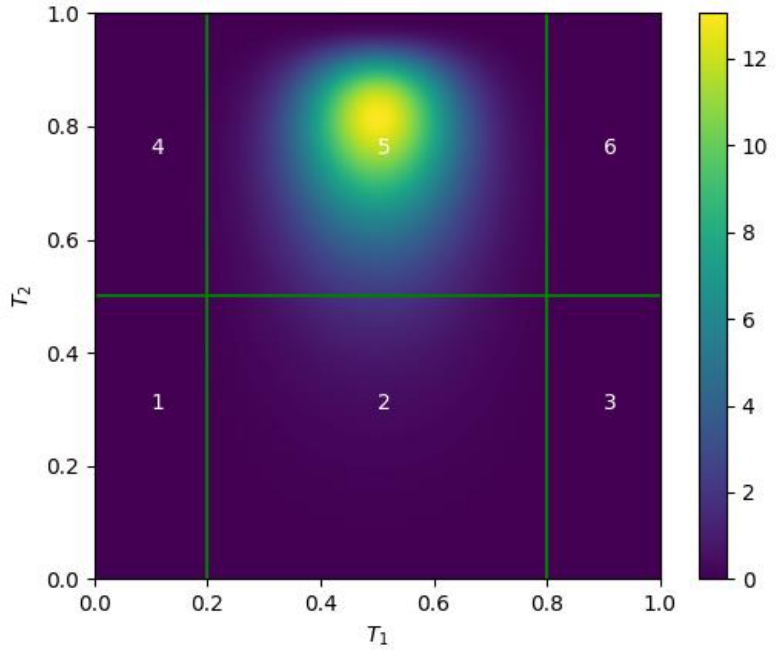

FIG 1: Joint Distribution Function for the two test statistics for a relatively high SNR

The joint probability distribution allows tuning of the change detection thresholds in a way that can be used to maximize the probability of detecting changes of interest. In the example of FIG 1, one would look for responses in regions 1,2,3,4 and 6. This applies in areas with a relatively high SNR.

Unfortunately, in reality, a radar scene will be composed of areas of varied SNR. In areas with a low SNR, for instance in radar shadow areas, the distribution is as in FIG 2.

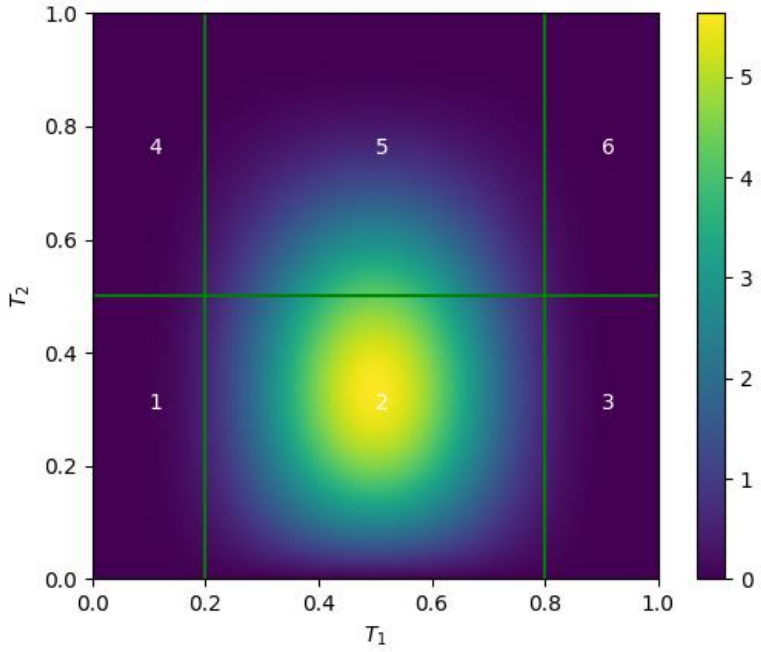

FIG 2: Joint Distribution Function in the case of low SNR

The observed center of mass of this unwanted noise-like signal is in region 2 and it thus makes sense to exclude region 2 from the space in which to automatically detect targets since anything detected in this region is likely a result of low SNR.

Detections in regions 4 and 6, where there is a large value for T_2 but extreme values for T_1most likely arise from different backscatter conditions since the correlation coefficient (which is sensitive to phase changes in the scatterers) indicates that the scatterers contributing to the return have not moved. These changes are usually not of interest.

Regions 1 and 3 provide ideal locations in which to detect changes of interest, while minimizing false alarms due to low SNR. In these regions, amplitude change detection is reinforced by coherent change detection. In the example of this paper, the change detection is carried out in regions 1 and 3.

We illustrate the method and compare with results using MIMOSA, a software package based upon [2]. Two SAR images, collected by TerraSAR-X and provided by the Deutschen Zentrums für Luft- und Raumfahrt (DLR), are shown in FIG 3 and FIG 4.

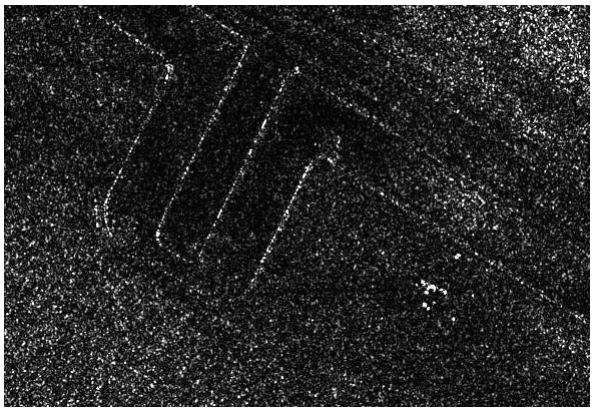

FIG 3: Primary SAR Image

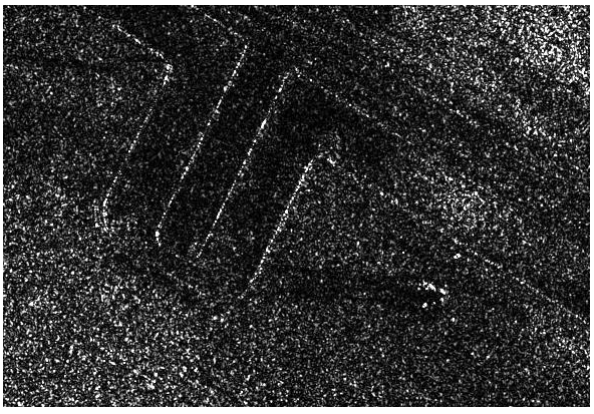

FIG 4: Secondary SAR Image

Change detection using both the MIMOSA software and the proposed method is shown in FIG 5 and FIG 6. Both methods work quite well though the MIMOSA software seems to detect more changes in the lower right portion of the image. The magenta colored changes correspond to scatterers that are in the primary image, but not in the secondary image while green indicates scatterers in the secondary image, but not in the primary. The MIMOSA detects twelve changes, while the proposed method detects six. Note that in both cases, singleton change detections (detections that span only a single pixel) have been eliminated. In the MIMOSA case, the

false alarm rate is set to half a percent; thus, given the number of pixels in the image, ~230,000, this should correspond to approximately 1200 false alarms which is clearly not the case. The fact that singleton detections have been eliminated only partially accounts this discrepancy, as there were only around 30 singleton detections. A conservative estimate of the false alarm rate for data processed with the proposed method yields a false alarm rate of 10e-5 which should yield 2 or three false alarms.

Without ground truth data, the performances of these methods cannot be quantitatively compared. Visual inspection does indicate change in the area highlighted by both change detection algorithms; however, what these changes correspond to is not known. The changes may relate to vehicle movement or they may relate to the use of equipment.

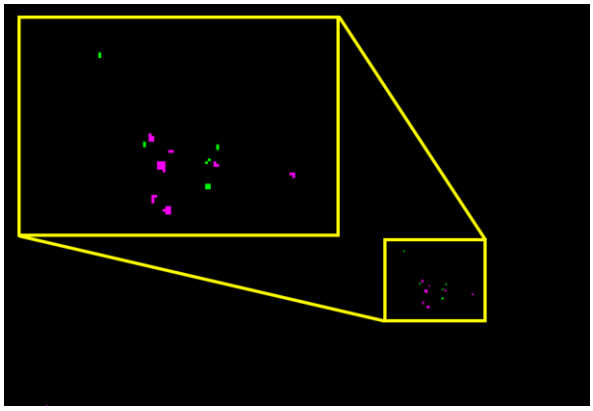

FIG 5: Change detection with MIMOSA software

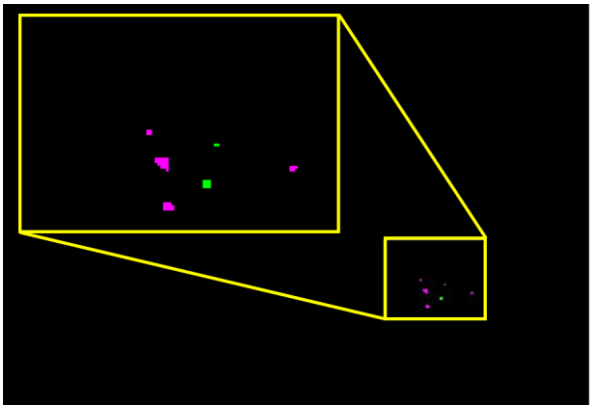

FIG 6: Change detection with proposed method

If it is a priori known that the area under examination is of relatively high SNR, then region 2 can be included in the space in which to detect change. Detections in this region make radar coherent change detection particularly sensitive as it is in this region that signatures of used vehicles tracks or slight orientation changes in equipment would appear.

The described approach can be made adaptive to the local SNR if it is estimated.

4. A MACHINE LEARNING ALGORITHM TO IMPROVE CHANGE DETECTION

Changes to due to environmental or natural effects need to be excluded from final change detection results. In this section, a machine learning approach is used to remove changes associated with water in the scene under analysis.

The approach proposes to use a subset of elements of $\widehat{\boldsymbol{R}}(m', n')$ as features in a supervised machine learning classification algorithm. Specifically, at each pixel (m', n'), a three-element feature vector, **x,** is defined as

$$\mathbf{x} = (x_1, x_2, x_3) = (R_{11}, R_{22}, \rho).$$

In supervised classification, *training data* are provided as exemplars for training the algorithm. These data are given in the form of a set of *N* labeled feature vectors within a spatial region of interest (ROI) for both water and non-water (background) pixels. FIG 7 illustrates the SAR imagery and the selection of training data for the example provided by this paper. The RGB image consists of the primary SAR (scaled between 0 and 1) image in the red, the secondary SAR image (scaled between 0 and 1) in green and the correlation coefficient in blue. The data used in this example are from Sentinel-1 imagery collected over an area chosen only because it contains many exemplary bodies of water

In general, maximum likelihood classification requires analysis of the statistics for each class of data. For simplicity, in this paper, each feature vector is assumed to follow a multivariate Gaussian distribution; an assumption somewhat validated by visual inspection of the scatter plots of features. Parameters of the probability density function for each class are estimated using the histogram of pixel values from the training ROIs.

After implementing the maximum likelihood detection algorithm and again removing singleton detections from water, one obtains the result illustrated in FIG 8. Implementation of this algorithm very clearly shows how one can readily exclude water-induced changes that would have been detected in the regions outlined in blue. The mask obtained by setting blue to zero and green to one can simply be applied to any of the statistical change detection outputs discussed in the previous section.

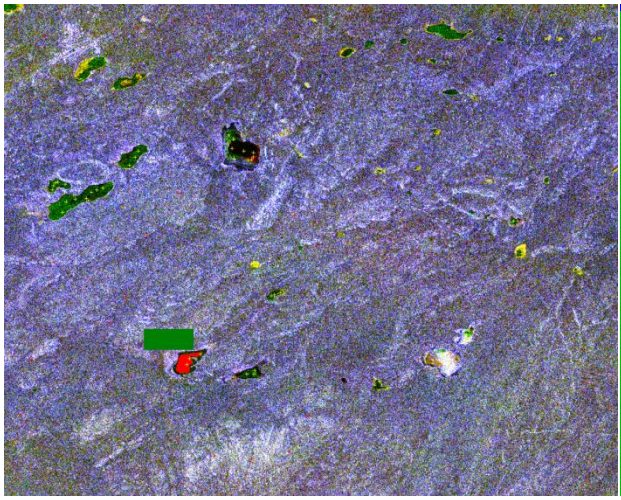

FIG 7: Training areas for water in red, not water in green

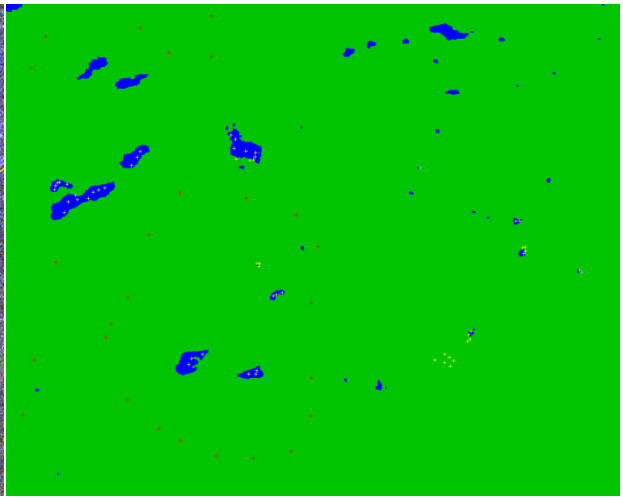

FIG 8: Results of classification. Red and yellow markers used denote samples used for validation

In future work, such a classifier could be generalized to identify not only whether change has occurred in a set of radar images, but also what kind of change has occurred. That is, it could be generalized to also do the work of the statistical change detection algorithms discussed in Section 3. As a specific example, these classes could be as outlined in Table 1.

Table 1: CHANGE-DETECTION CLASSES

Class Name	**Class Name**	**Class Name**
Unchanged	Unchanged	Unchanged
Change	Coherent Change	Reoriented object
		Track used
		Low SNR
		Environmental
	Amplitude Change	New object
		Speckle
		Environmental

5. CONCLUSION

This paper has provided an introduction to automated change detection methods for radar imagery. These automatable methods have become ever more important as the volume of data continues to grow. While the methods will probably not replace a human analyst, they show great potential to assist the analyst. The paper introduced two statistical change detection methods already published in the literature, and in one case already implemented in software. It then proposed a variation on these methods that shows good potential to improve these methods. Finally, the paper introduced a machine learning algorithm with the specific aim of creating a false change detection mask thereby facilitating the work of an analyst. It is expected that the methods presented in this paper will be adapted, further developed or fine-tuned to a state where they can provide operational value.

REFERENCES

[1] Conradsen, K., Nielsen, A. A., & Skriver, H. Determining the points of change in time series of polarimetric SAR data, IEEE Trans. Geoscience and Remote Sensing **54** 5 (2016) 3007-3024.

[2] Quin, G., Pinel-Puyssegur, B., Nicolas, J. M., & Loreaux, P., MIMOSA: An automatic change detection method for SAR time series, IEEE Transactions on Geoscience and Remote Sensing **52** 9 (2014) 5349-5363.

[3] Cui, S., Schwarz, G. & Datcu, M., A comparative study of statistical models for multilook SAR images, IEEE Geoscience and Remote Sensing Letters **11** 10 (2014) pp.1752-1756.

[4] Gierull, C. H., Statistical analysis of multilook SAR interferograms for CFAR detection of ground moving targets. IEEE Transactions on Geoscience and Remote Sensing **42** 4 (2004) 691-701.

[5] Beauchemin, M., Thomson, K. P., & Edwards, G., The ratio of the arithmetic to the geometric mean: a first-order statistical test for multilook SAR image homogeneity, IEEE Transactions on Geoscience and Remote Sensing **34** 2 (1996) 604-606.

[6] Nielsen, A. A., Conradsen, K., Skriver, H., & Canty, M. J., "Change detection in a series of Sentinel-1 SAR data", 9th International Workshop on the Analysis of Multitemporal Remote Sensing Images (MultiTemp), IEEE, Bruges (2017).

[7] Sikaneta, I., Gierull, C., & Chouinard, J. Y., "Metrics for SAR-GMTI based on eigen-decomposition of the sample covariance matrix", 2003 Proceedings of the International Conference on Radar, IEEE, Adelaide (2003).

[8] Gradshteyn, I. S. & Ryzhik, I. M., "Table of Integrals, Series and Products", Academic Press, New York, sixth edition, 2000.